Theor. Appl. Climatol. (2004)
DOI 10.1007/s00704-004-0049-4

Theoretical and Applied Climatology
Printed in Austria

[1] Hadley Centre for Climate Prediction, Research, Met Office, Exeter, UK
[2] Department of Meteorology, University of Reading, Reading, Berks, UK
[3] Centre for Ecology and Hydrology, Wallingford, Oxon, UK

# Amazonian forest dieback under climate-carbon cycle projections for the 21st century

**P. M. Cox**[1], **R. A. Betts**[1], **M. Collins**[2], **P. P. Harris**[3], **C. Huntingford**[3], and **C. D. Jones**[1]

With 10 Figures

Received March 28, 2003; revised August 16, 2003; accepted October 9, 2003
Published online April 27, 2004 

**Summary**

The first GCM climate change projections to include dynamic vegetation and an interactive carbon cycle produced a very significant amplification of global warming over the 21st century. Under the IS92a "business as usual" emissions scenario $CO_2$ concentrations reached about 980 ppmv by 2100, which is about 280 ppmv higher than when these feedbacks were ignored. The major contribution to the increased $CO_2$ arose from reductions in soil carbon because global warming is assumed to accelerate respiration. However, there was also a lesser contribution from an alarming loss of the Amazonian rainforest. This paper describes the phenomenon of Amazonian forest dieback under elevated $CO_2$ in the Hadley Centre climate-carbon cycle model.

## 1. Introduction

About half of the current anthropogenic emissions of carbon dioxide are being absorbed by the ocean and by land ecosystems (Schimel et al., 1996). The processes involved are known to be sensitive to climate. Temperature affects the solubility of carbon dioxide in sea-water and the rate of terrestrial and oceanic biological processes. Vegetation also responds directly to elevated $CO_2$ through increased photosynthesis and reduced transpiration (Sellers et al., 1996; Field et al., 1995), and may also change its structure and distribution in response to any associated climate change (Betts et al., 1997). The biosphere therefore has great potential to produce a feedback on the climate change due to anthropogenic $CO_2$ emissions. However, simulations carried out with General Circulation Models (GCMs) have generally neglected the coupling between the climate and the biosphere. Instead, vegetation distributions have been static and atmospheric concentrations of $CO_2$ have been prescribed based on results from simple carbon cycle models, which neglect the effects of climate change.

Recently some groups have begun to include representations of the carbon cycle within GCMs (Friedlingstein et al., 2001; Cox et al., 2001). The first climate change projection to include both an interactive carbon cycle and dynamic vegetation was carried out at the Hadley Centre, and this showed a significant acceleration of $CO_2$ increase and climate change arising from the additional feedback loops (Cox et al., 2000). Under the IS92a "business as usual" emission scenario the Hadley Centre coupled-climate carbon cycle model produced a $CO_2$ concentration of about 980 ppmv by 2100, compared to about

**Table 1.** Change in carbon stores from 1860 to 2100 from the fully interactive climate-carbon cycle projection (''Online'' run), and a run in which there were no climate effects on the carbon cycle (''Offline'' run). Changes in South American soil and vegetation carbon are shown for comparison

| | ''Offline'' | ''Online'' |
|---|---|---|
| $CO_2$ emissions (GtC) | 1883 | 1883 |
| Atmospheric Change (GtC) | 883 | 1486 |
| Ocean Storage (GtC) | +367 | +495 |
| Global Land Storage (GtC) | +633 | −98 |
| S. American Soil Carbon Storage (GtC) | +76 | −55 |
| S. American Vegetation Carbon Storage (GtC) | +64 | −73 |

700 ppmv when climate effects on the carbon cycle were excluded. This resulted in an amplification of global warming from about 4 K to about 5.5 K.

Table 1 summarises the change in carbon stores from 1860–2100 with and without carbon cycle feedbacks (''online'' and ''offline'' experiments respectively). In the offline case 1000 GtC of the integrated emissions are absorbed by the land (633 GtC) and oceans (367 GtC). However, once climate effects on the carbon cycle are included land storage *decreases* by about 98 GtC over the 1860–2100 period. The net change in land carbon storage of 731 GtC is only slightly offset by increased oceanic uptake of 128 GtC because of higher $CO_2$. As a result, the fully coupled ''online'' run has 731−128 = 603 GtC more atmospheric carbon by 2100, which is equivalent to about 280 ppmv (see Fig. 1a).

Figure 1 shows the reason for this acceleration of climate change. In the absence of climate change (dashed lines) the land takes up carbon as a result of $CO_2$-fertilisation of growth, saturating at a global land carbon sink of about 5.5 GtC $yr^{-1}$. The additional terrestrial carbon is stored in both vegetation and soils (respective increases of about 223 GtC and 410 GtC from 1860 to 2100). However, once climate-carbon cycle feedbacks are included (continuous lines in Fig. 1) the historical land carbon sink is strongly suppressed, and ultimately flips to be a global land carbon source from the middle of the 21st century (after the atmospheric $CO_2$ concentration passes about twice its pre-industrial value). The negative impacts of climate change are most evident in the soil carbon store which releases about 150 GtC by 2100, rather than storing 410 GtC.

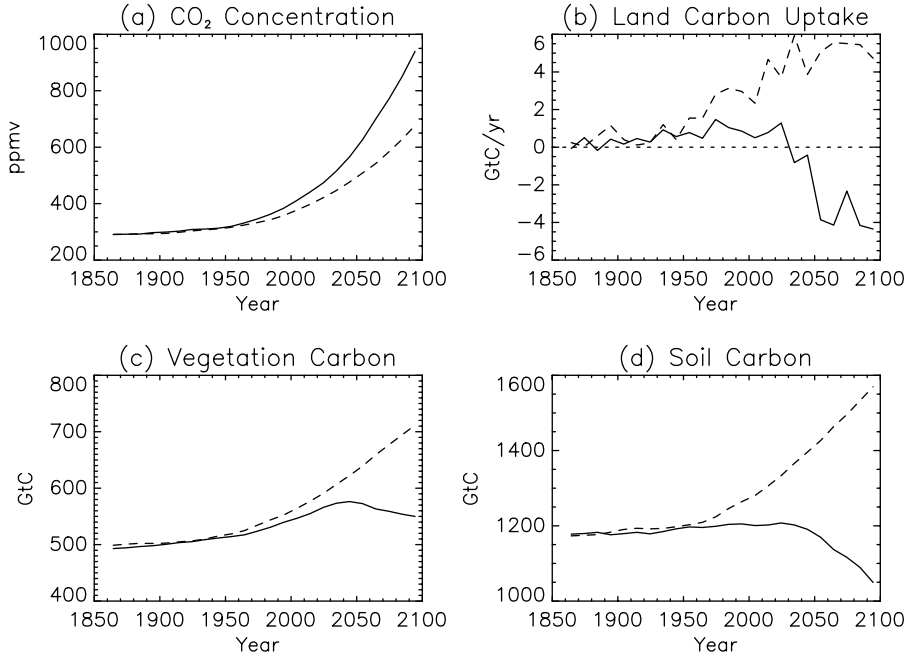


**Fig. 1.** Impact of climate-carbon cycle feedbacks on projections of (**a**) atmospheric $CO_2$ concentration, (**b**) global land carbon uptake, (**c**) global vegetation carbon and (**d**) global soil carbon. The continuous line represents the fully coupled climate-carbon cycle run and the dashed line is from the run without climate effects on the carbon cycle

This response of soil carbon to climate change is consistent with the standard assumption that decomposition occurs more rapidly in warmer conditions (Jenkinson et al., 1991). The Hadley Centre Dynamic Global Vegetation Model, ''TRIFFID'', updates a single soil carbon store based on litterfall inputs from vegetation, and soil respiration (i.e. decomposition) losses which are dependent on soil temperature and soil moisture, as well as the size of the soil carbon pool (Cox, 2001). Specific soil respiration (i.e. the rate per unit of soil carbon) is assumed to double with every 10 K increase in temperature (i.e. $q_{10} = 2$), which represents a central estimate of the temperature sensitivity based on laboratory and field measurements (Raicha and Schlesinger, 1992). Doubts have been raised about the longer-term response of soil decomposition to warming (Giardina and Ryan, 2000), but interannual $CO_2$ variability suggests that $q_{10} = 2$ is a good assumption at least out to the decadal timescale (Jones and Cox, 2001).

In soil models of this type, warming enhances the respiration loss term, reducing the size of the respiring soil carbon pool until the absolute respiration flux (i.e. specific respiration rate $\times$ respiring soil carbon) once again balances the litter inputs. Thus even such simple models of soil carbon dynamics produce ''acclimation'' of the absolute soil respiration flux to higher temperatures, but they do this at the cost of dynamic reductions in the size of the respiring carbon pool. As a result the land becomes an overall carbon source at high $CO_2$, provided a few simple conditions are met (Cox et al., 2001).

Figure 1c shows that climate change also has a negative impact on carbon storage in vegetation, resulting in a reduction of global biomass from the middle of the 21st century onwards. As a consequence the fully coupled run accumulates only about 55 GtC of vegetation carbon from 1860 to 2100, rather than about 223 GtC when climate effects on the carbon cycle are excluded. The reduction in vegetation carbon is dominated by South America which loses about 73 GtC of biomass over the 1860–2100 period (see lowest row of Table 1). Cox et al. (2000) describe this as due to climate-driven ''dieback'' of the rainforest, resulting from regional drying in Amazonia. Such a loss of rainforest would have catastrophic impacts on the biodiversity and ''ecosystem services'' of Amazonia, similar to those anticipated under the most extreme scenarios of direct human deforestation (Nepstad et al., 1999). It is therefore vital that we estimate the risk of climate-driven Amazonian forest dieback, and identify any relevant thresholds in the climate-carbon cycle system.

This paper serves as an overview of collaborative work which has been carried out to analyse aspects of the Hadley Centre's climate-carbon cycle model response in Amazonia. Subsequent papers in this LBA special issue will deal specifically with biophysical vegetation feedbacks (Betts et al., 2004), improvements to the parametrization of land-atmosphere $CO_2$ fluxes (Harris et al., 2004), and the impacts of these improvements plus errors in the GCM control climate on the dieback phenomenon (Huntingford et al., 2004).

The next section describes the Hadley Centre climate-carbon cycle GCM, and Section 3 compares its simulation of Amazonian climate and vegetation to observations. The projections of climate change are described in Sections 4 and 5, the vegetation response is discussed in Section 6 and the related biophysical feedbacks are summarised in Section 7 (see Betts et al. (2004) for further details). Section 8 discusses outstanding questions, and suggests the additional research required to address these.

## 2. Model description

The climate-carbon cycle GCM used in this study (''HadCM3LC'') is identical to that used by Cox et al. (2000) and described in detail elsewhere (Cox et al., 2001). The GCM is based on the third Hadley Centre coupled ocean-atmosphere model, HadCM3 (Gordon et al., 2000), coupled to an ocean carbon cycle model (''HadOCC'') and a dynamic global vegetation model (''TRIFFID''). The atmospheric physics and dynamics are identical to those used in HadCM3, with a longitude–latitude grid of $3.75^\circ \times 2.5^\circ$ and 19 levels in the vertical. As in HadCM3, runoff generated on the land is routed to specified river outflow points using a discretised map of the largest river basins. The additional computational expense of including an interactive carbon cycle made it necessary to reduce the ocean horizontal resolution from the

standard $1.25° \times 1.25°$ in HadCM3, to a $2.5° \times 3.75°$ grid congruent with the atmospheric model. Heat and freshwater flux-adjustments were used in the ocean component to prevent the development of climate errors which might compromise the simulation of the land and ocean carbon cycles. Comparisons between HadCM3 and HadCM3LC have shown very similar rates and patterns of warming under the same scenario (and with fixed vegetation), despite the use of flux-adjustments in the latter.

### *2.1 Ocean carbon cycle*

HadOCC simulates the movements of carbon within the ocean system, including exchange of carbon dioxide gas with the atmosphere, the circulation of dissolved inorganic carbon (known as DIC or $tCO_2$) within the ocean, and the cycling of carbon by the marine biota. The principle components of the model are handled as tracers within the physical ocean model. They are: (nitrogenous) nutrient, phytoplankton, zooplankton, detritus, $tCO_2$ and alkalinity.

The air-to-sea flux of carbon dioxide is calculated using standard parametrizations:

$$F_{AS} = K(c_a - c_o) \quad (1)$$

where $c_a$ and $c_o$ are respectively the partial pressures of $CO_2$ in the atmosphere and ocean at a given location. $K$ parametrizes the effect of the windspeed on the gas transfer velocity, using the formulation of Wanninkhof (1992). Winds are obtained from the atmospheric model. The partial pressure of $CO_2$ in the surface waters is determined by solving equations representing the seawater acid-base system. The expressions for the dissociation constants of carbonic acid, hydrogen carbonate, boric acid and water and for the solubility of $CO_2$ in seawater are taken from DOE (1994). Using the salinity dependent boron concentration of Peng (1987), the acid base system is solved using the method of Bacastow and Keeling (1981) to yield the concentration of carbonic acid and hence the partial pressure of $CO_2$. The temperature and salinity values used in these calculations are the local values from the ocean model.

The biological component of HadOCC is an explicit ecosystem model consisting of the four components; nutrient (assumed to be nitrate), phytoplankton, zooplankton and (sinking) detritus (Palmer and Totterdell, 2001). The complexity of the model was restricted to just four compartments in order for it to be economical enough for use in long integrations. This means that the behaviours of many different species and size-fractions are aggregated into a single component for each of phytoplankton and zooplankton. The model calculates the flow of nitrogen between the four components of the ecosystem at each grid box, and also computes the associated transfers of carbon and alkalinity. The carbon flows have no direct effect on the behaviour of the ecosystem as growth of phytoplankton is not limited by availability of carbon.

The phytoplankton population changes as a result of the balance between growth, which is controlled by light level and the local concentration of nutrient, and mortality, which is mostly as a result of grazing by zooplankton. Detritus, which is formed by zooplankton excretion and by phyto- and zooplankton mortality, sinks at a fixed rate and slowly remineralises to reform nutrient and dissolved inorganic carbon. Thus both nutrient and carbon are absorbed by phytoplankton near the ocean surface, pass up the food chain to zooplankton, and are eventually remineralised from detritus in the deeper ocean.

### *2.2 Land carbon cycle*

TRIFFID defines the state of the terrestrial biosphere in terms of the soil carbon, and the structure and coverage of five plant functional types (Broadleaf tree, Needleleaf tree, $C_3$ grass, $C_4$ grass and shrub) within each model gridbox. The areal coverage, leaf area index and canopy height of each type are updated based on a carbon balance approach, in which vegetation change is driven by net carbon fluxes calculated within the "MOSES 2" land surface scheme (Essery et al., 2003). MOSES 2 is a tiled version of the land surface scheme described by Cox et al. (1999), in which a separate surface flux and temperature is calculated for each of the land-cover types present in a GCM gridbox. In its standard configuration, MOSES 2 recognises the five TRIFFID vegetation types plus four non-vegetation land-cover types (bare soil, inland water, urban areas and land ice). Carbon fluxes for each of the vegetation types are derived using the

coupled photosynthesis-stomatal conductance model developed by Cox et al. (1998), which utilises existing models of leaf-level photosynthesis in $C_3$ and $C_4$ plants (Collatz et al., 1991, 1992). Plant respiration is broken-down into a growth component, which is proportional to the photosynthetic rate, and a maintenance component which is assumed to increase exponentially with temperature ($q_{10} = 2$). The resulting rates of photosynthesis and plant respiration are dependent on both climate and atmospheric $CO_2$ concentration. Therefore, with this carbon-balance approach, the response of vegetation to climate occurs via climate-induced changes in the vegetation to atmosphere fluxes of carbon.

The land-atmosphere fluxes are calculated by MOSES 2 on every 30 minute GCM timestep and time-averaged before being passed to TRIFFID every 10 days. TRIFFID allocates the average net primary productivity over this coupling period into the growth of the existing vegetation (leaf, root and wood biomass), and to the expansion of the vegetated area in each gridbox. Leaf phenology (bud-burst and leaf drop) is updated on an intermediate timescale of 1 day, using accumulated temperature-dependent leaf turnover rates. After each call to TRIFFID the land surface parameters required by MOSES 2 (e.g. albedo, roughness length) are updated based on the new vegetation state, so that changes in the biophysical properties of the land surface, as well as changes in terrestrial carbon, feedback onto the atmosphere. The land surface parameters are calculated as a function of the type, height and leaf area index of the vegetation. Full details on TRIFFID are given by Cox (2001).

## 3. Simulation of the pre-industrial climate and vegetation of Amazonia

Before any climate projections could be carried out HadCM3LC needed to be brought to a ''pre-industrial'' equilibrium state. A good approximation to equilibrium is particularly important for the carbon cycle because land and ocean carbon sinks are only a small fraction of the gross surface-atmosphere $CO_2$ exchanges, so even a relatively small model imbalance can swamp the signal of net carbon uptake. The model spinup was carried out as a multistage process involving a long ocean-only run (2000 model years), and coupled runs (150 model years in total) with fixed $CO_2$ of 290 ppmv to derive the equilibrium vegetation state consistent with the model's pre-industrial climate (Cox et al., 2001). Once the long-term net land-atmosphere and ocean-atmosphere carbon fluxes were close to zero the atmospheric $CO_2$ was let free to respond to variability in the model's global carbon cycle (assuming zero pre-industrial anthropogenic $CO_2$ emissions). The coupled climate-carbon cycle model was then integrated for 100 years so that its mean state and variability could be diagnosed.

Figure 2 and Fig. 3 compare the spatial and seasonal variations from this pre-industrial run to climate and vegetation observations for current day Amazonia (New et al., 1999; Loveland et al., 2000). A completely clean comparison is not possible because of the absence of accessible pre-industrial observations. However, it is still a useful validation exercise since pre-industrial to present day changes are generally much smaller than projected changes over the 21st century (see Section 4).

The Hadley Centre atmospheric models have typically been amongst the more accurate GCMs over Amazonia (see for example Gedney et al., 2000), largely because modelling this region has been a long-standing priority at the Met Office (Lean and Rowntree, 1993, 1997). However, deficiencies in the simulation are still very apparent. Figure 2 shows maps of the annual mean rainfall, temperature and vegetation cover over South America. The model correctly produces a rainfall maximum in the west, and minima in the east and over the Andes. However, rainfall is generally underestimated especially along the north-east coastline (a common problem in GCMs). The black boxes on the maps of Fig. 2 represent the definition of Amazonia for the purposes of calculating area mean values (70° W–50° W, 15° S–0° N). This region has been selected to maintain consistency with previous studies (Gedney et al., 2000), but its definition is unlikely to affect the qualitative conclusions drawn in this paper. The area mean rainfall over this box is underestimated in the model by about 20% ($4.63\,\mathrm{mm\,day^{-1}}$ as opposed to $5.78\,\mathrm{mm\,day^{-1}}$, New et al., 1999), which has implications for the timing of Amazonian dieback (Huntingford et al., 2004). Annual mean temperature is much more accurately captured with patterns and

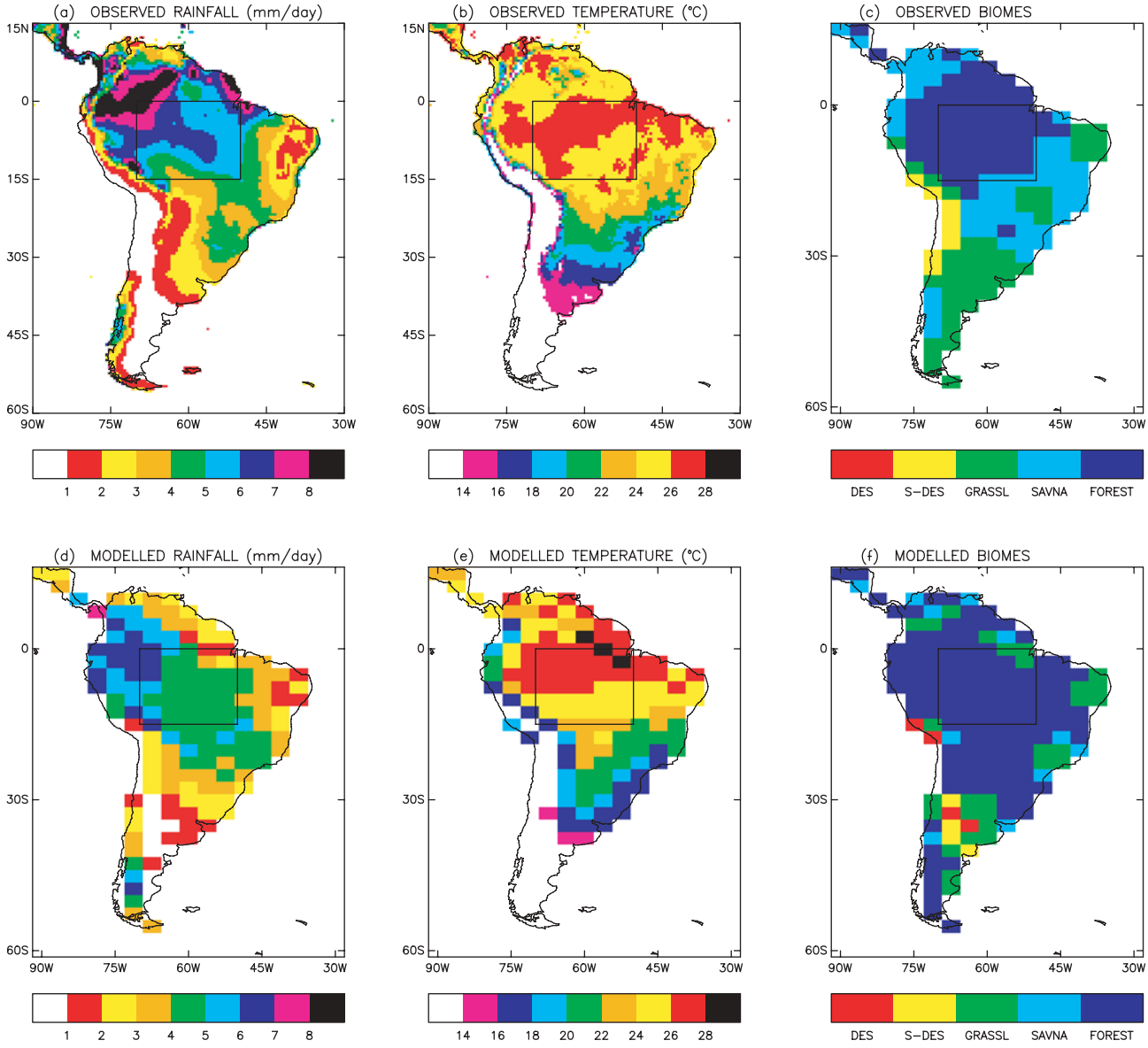


**Fig. 2.** Rainfall, screen-level air temperature and biome distributions over South America from observational datasets (**a**, **b**, **c**) and the model simulation of the pre-industrial state (**d**, **e**, **f**). Climate observations are from New et al. (1999) and the biome distribution is derived from Loveland et al. (2000)

magnitudes well reproduced (compare panels (b) and (e) of Fig. 2). The modelled mean air temperature over the Amazon box (25.90 °C) is remarkably close to the observational estimate of 25.94 °C (New et al., 1999).

Panels (c) and (f) of Fig. 2 compare modelled and observed biome distributions over South America. TRIFFID models the fractional area covered by each of its 5 plant functional types, so these biomes are derived by post-processing using the rules summarised in Table 2. Similar processing of the IGBP land-cover map (previously converted to TRIFFID PFTs), yields panel (c). The model does a reasonable job of reproducing the locations of the grasslands, deserts and semi-deserts of South America, and also correctly simulates tropical forests in the Amazon box. However, trees are regularly overpredicted in the savanna regions. Only a fraction of this error can be attributed to the neglect of direct human deforestation in the model. The remaining error is most likely to be due to the

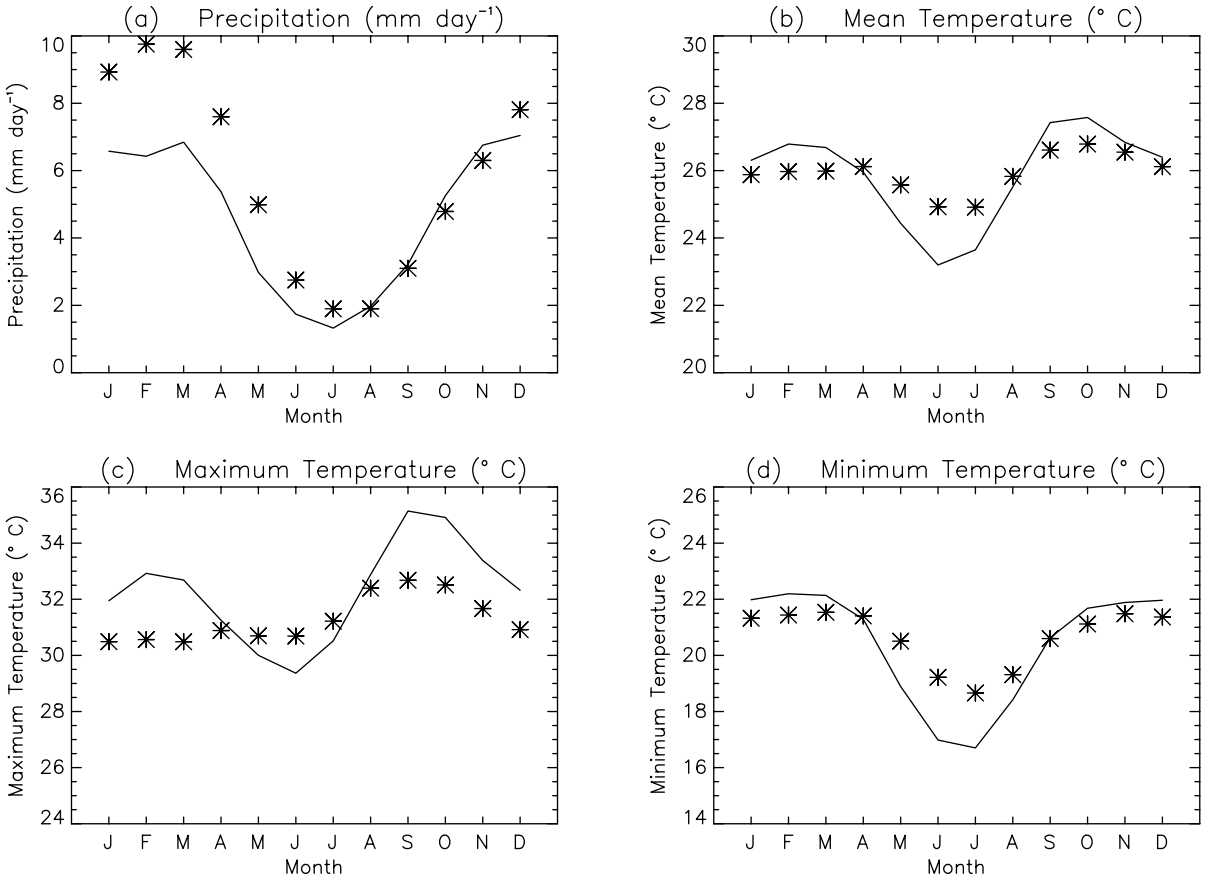


**Fig. 3.** Seasonal cycle in (**a**) rainfall, (**b**) air temperature, (**c**) daily maximum air temperature and (**d**) daily minimum air temperature, over the Amazon box (see previous figure). The pre-industrial simulation is shown by the continuous line and the symbols represent the observational climatology (New et al., 1999)

**Table 2.** Rules used to convert TRIFFID vegetation fractions into Biome types as used in Fig. 2

| Biome type | TRIFFID area fractions | | |
|---|---|---|---|
| | Total vegetation | Total tree | Bare soil |
| Forest | | $\geq 0.5$ | |
| Savanna | $\geq 0.5$ | $\geq 0.2$, $<0.5$ | |
| Grassland | $\geq 0.5$ | $<0.2$ | |
| Semi-desert | $\geq 0.2$, $<0.5$ | | |
| Desert | | | $>0.8$ |

absence of fire-disturbance processes in this version of TRIFFID. A forest fire model is under-development to correct this deficiency, but for the time-being it is worth noting that TRIFFID has a tendency to *overestimate* rather than underestimate the robustness of tropical forests to climate variation.

Figure 3 compares the seasonal cycles in rainfall, and mean, maximum and minimum temperature, to an observational dataset (New et al., 1999). The error in the annual mean rainfall is seen to be largely due to an underestimate of wet season rainfall in northern hemisphere winter (Dec–Feb) and spring (March–May). The minimum rainfall is well captured, although the dry season appears a month early. However, the recovery from the dry season appears to be well reproduced by the model.

Although the observed annual mean daily maximum and minimum temperatures (31.3 °C and 20.7 °C respectively) are closely matched by the model (32.3 °C and 20.4 °C respectively), this is inspite of the tendency of the model to overestimate seasonal temperature variation. Mean, maximum and minimum temperatures all seem to differ too much between wet and dry seasons, perhaps suggesting a deficiency in cloud cover. However, more definite conclusions on this will need to await further analysis of both the model and the observational dataset (for which significant interpolation of sparse

available observations is likely to have been required).

Overall, this validation exercise has served to reinforce the view that HadCM3LC has at least comparable performance in South America to most other coupled ocean-atmosphere GCMs, even though these typically exclude the additional complexities of dynamic vegetation. Nevertheless, the deficiencies outlined here will need to be borne in mind when assessing the climate sensitivity of the model in subsequent sections.

## 4. Projection of 21st century climate change in Amazonia

Figure 4 shows maps of the change in climate and land carbon (between 2000 and 2100) from the GCM experiment reported by Cox et al. (2000), which used the fully interactive carbon cycle with IS92a $CO_2$ emissions. Other greenhouse gas concentrations were prescribed as a function of year based on offline atmospheric chemistry calculations. Sulphate aerosols were not included in this experiment. Subsequent runs have shown that the cooling effects of anthropogenic and volcanic aerosols act to improve the simulation of the historical $CO_2$ rise, and also slightly delay the sink-to-source transition in the terrestrial carbon cycle (Jones et al., 2003). However, these important climatic forcings do not qualitatively change the projected impacts on the Amazonian forest, so here we choose to analyse the original Cox et al. (2000) avoiding the additional complexities of the atmospheric sulphur cycle.

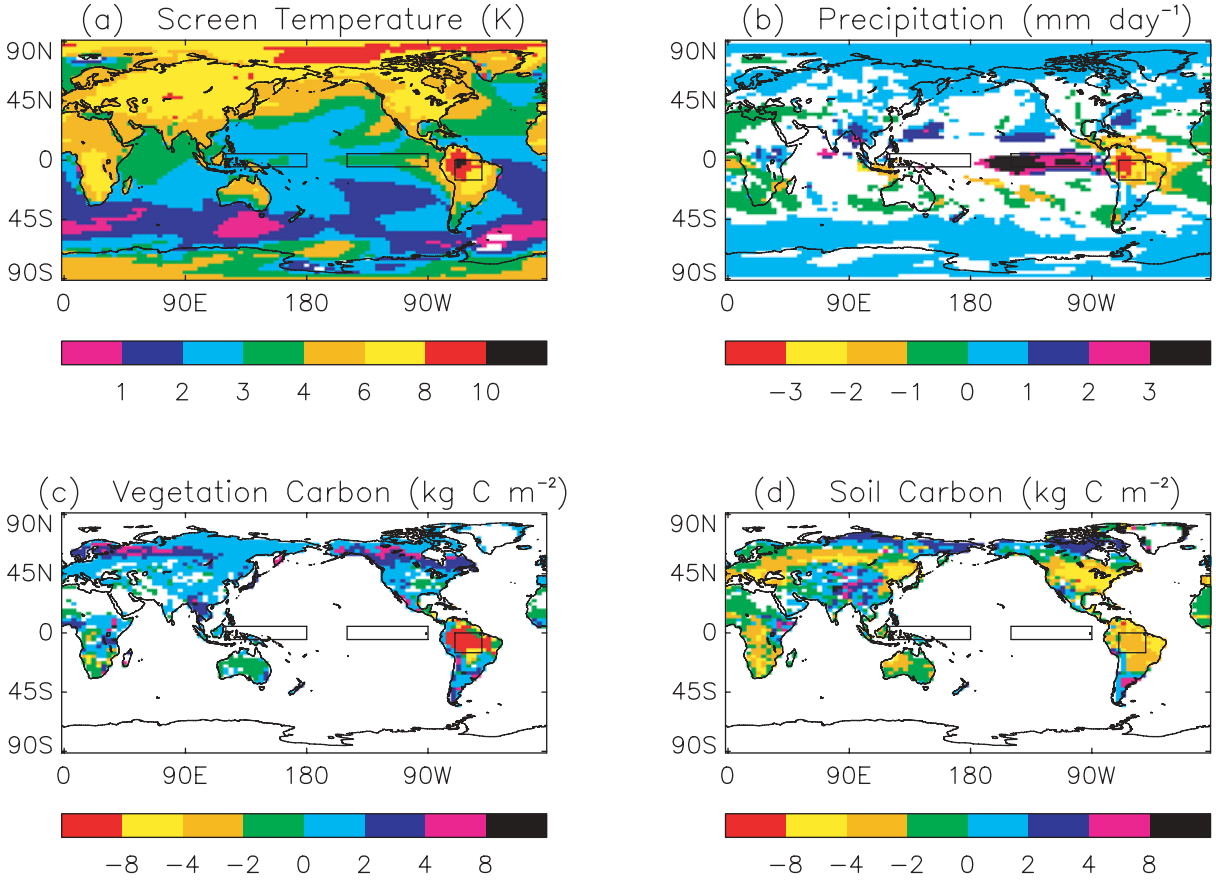


**Fig. 4.** Maps of changes in climate and land carbon storage over the 21st century from the fully coupled climate-carbon cycle projections. (**a**) Screen temperature, (**b**) precipitation, (**c**) vegetation carbon and (**d**) soil carbon. These maps were calculated as the differences between the means for the 2090s and the 1990s. Only areas for which the projected change is greater than 95% significant (according to a paired student t-test) are shown. In each map the box over South America represents the definition of Amazonia for the purposes of this study (70° W–50° W, 15° S–0° N), while the boxes over the Pacific show the NINO3 region (150° W–90° W, 5° S–5° N), and the western Equatorial Pacific region as used in Fig. 5 (120° E–180° E, 5° S–5° N)

The global mean warming of about 5.5 K by 2100 is consistent with an equilibrium climate sensitivity to doubling $CO_2$ of about 3.2 K, which is near the centre of the range quoted by the IPCC (1.9–5.2 K, IPCC (2001)). Figure 4a shows a significant land-sea temperature contrast implying a greater potential for impacts on terrestrial ecosystems. The extra warming over land is partly due to $CO_2$-induced stomatal closure which suppresses evaporative cooling at high $CO_2$ (Cox et al., 1999), but there are also important contributions from cloud feedbacks (Williams et al., 2001). As is usual in GCMs, there is a tendency for the warming to be greatest in the high northern latitudes due to snow and sea-ice albedo feedbacks. However, the most severe warming is actually seen in western Amazonia where temperatures are projected to rise by more than 10 K by 2100. This area of extreme temperatures is concident with the region of maximum rainfall reduction (Fig. 4b), suffering a decrease of more than 3 mm day$^{-1}$ between 2000 and 2100. There is a very significant tendency to warm and dry over most of the northern half of South America.

Vegetation carbon increases in the forested regions of the northern hemisphere mostly as a result of $CO_2$-fertilisation of photosynthesis (Fig. 4c). Warming also leads to a longer snow-free period and therefore an extended growing season in the boreal regions. Tropical ecosystems fair less well from the projected changes as the warming generally leads to temperatures which are above the optimum for photosynthesis. Once again the most marked change in vegetation carbon is in Amazonia, where biomass drops by more than 8 kg C m$^{-2}$. The red regions of Fig. 4c roughly denote the area of ''Amazonian forest dieback''. Figure 4 shows that the loss of soil carbon is much more widespread, with only the far northern tundra regions accumulating soil carbon between 2000 and 2100. The tendency to lose soil carbon elsewhere is an inevitable consequence of the assumption that decomposition rate continues to increases with temperature, while photosynthesis saturates at high $CO_2$ (Jenkinson et al., 1991; Cox et al., 2001).

Table 3 summarises the area mean changes over the Amazon box (as marked on Fig. 4) and constrasts these to global mean changes. Amazonian temperature rises by more than 9 K over the 21st century, and rainfall drops by an alarming 64%. Together these changes lead to a 78% loss in vegetation carbon and a 72% loss in soil carbon. By contrast, over the same period the global mean temperature rises by about 4 K and rainfall increases by 3%. Global vegetation carbon increases by about 10 GtC despite the large losses in South America, but global soil carbon decreases by about 155 GtC. The carbon loss in the Amazon basin of about 50 GtC accounts for 23 ppmv of the total $CO_2$ increase of about 600 ppmv over the 21st century, or about a third of the total terrestrial carbon reduction of 145 GtC.

Table 4 serves to separate the causes of these changes in land carbon, by comparing the fully coupled ''online'' run to the ''offline'' run in which there were no climate effects on the carbon cycle. The online and offline runs were previously shown in Fig. 1 as the continuous and dashed lines respectively. In the absence of climate-carbon cycle feedbacks direct $CO_2$ effects lead the Amazon box to accumulate about 10 GtC each in vegetation and soil, which is a small contribution to the global terrestrial carbon

**Table 3.** Mean climate and land carbon storage from the fully interactive climate-carbon cycle projection for the decades of the 1990s (left two columns) and the 2090s (right two columns). Values for Amazonia are contrasted with global mean values (land plus ocean). For the purpose of this study Amazonia is defined as the longitude–latitude box 70° W–50° W, 15° S–0° N

| | 1990s | | 2090s | |
|---|---|---|---|---|
| | Globe | Amazonia | Globe | Amazonia |
| Screen Temperature (K) | 288.0 | 301.4 | 292.1 | 310.6 |
| Precipitation (mm day$^{-1}$) | 2.96 | 4.56 | 3.05 | 1.64 |
| Evaporation (mm day$^{-1}$) | 2.96 | 3.14 | 3.05 | 1.20 |
| Vegetation Carbon (GtC) | 539.5 | 45.6 | 549.7 | 10.1 |
| Soil Carbon (GtC) | 1204.5 | 19.8 | 1049.2 | 5.5 |

**Table 4.** Change in mean climate and land carbon storage (2090s–1990s) from the fully interactive climate-carbon cycle projection (''Online'' run), and a run in which there were no climate effects on the carbon cycle (''Offline'' run). Values for Amazonia are contrasted with land mean values

| | ''Offline'' | | ''Online'' | |
|---|---|---|---|---|
| | Globe | Amazonia | Globe | Amazonia |
| Δ Screen Temperature (K) | 0.3 | 0.9 | 4.1 | 9.2 |
| Δ Precipitation (mm day$^{-1}$) | 0.0 | −0.1 | 0.1 | −2.9 |
| Δ Evaporation (mm day$^{-1}$) | 0.0 | −0.25 | 0.1 | −1.9 |
| Δ Vegetation Carbon (GtC) | 159.0 | 10.3 | 10.2 | −35.6 |
| Δ Soil Carbon (GtC) | 304.9 | 10.3 | −155.3 | −14.3 |

accumulation of about 464 GtC. The coupled online run turns both these accumulations into the previously mentioned losses over the globe and the Amazon box of 145 GtC and 50 GtC, due to the negative impacts of climate change on land carbon storage. Climate-carbon cycle feedbacks therefore result in a net loss of about 610 GtC over the 21st century from global vegetation and soils, of which the Amazon box contributes about 70 GtC or 11% (this region accounts for just over 2% of the global land area). This is to be compared to a difference in atmospheric $CO_2$ at 2100 of about 600 GtC between the online and offline runs (see Table 1).

We conclude this section by recognising that Amazonian dieback provides a small but significant contribution to the climate-carbon cycle feedback reported by Cox et al. (2000). Carbon losses in the Amazon box account for about a tenth of the amplification of $CO_2$ by 2100 (comparing online and offline runs), and about one third of the total terrestrial carbon losses projected for the 21st century in the coupled (online) run. Vegetation and carbon losses in Amazonia are associated with the areas of most extreme warming and drying within the model. The next section discusses this pattern of climate change and its possible relationship to the El Niño Southern Oscillation (ENSO).

## 5. Climate change and ENSO

Model projections of 21st century climate differ most markedly at small scales, implying significant uncertainty in regional climate change and its impacts. Nevertheless, some common features do emerge from GCM patterns of climate change (IPCC, 2001). The amplification of high latitude warming by snow and sea-ice albedo feedbacks is almost universally seen in GCM simulations. However, there are other regional details which are agreed upon by significant subsets of GCMs, such as the tendency for mid-latitude continents to dry in summer under global warming. The Third Assessment report of the IPCC also states that ''many models show a mean El Niño-like response in the tropical Pacific, with the central and eastern equatorial Pacific sea surface temperatures projected to warm more than the western Pacific and with a corresponding mean eastward shift of precipitation'' (IPCC (2001), Section F.7, p. 73). Returning to Fig. 4 note that this statement is broadly consistent with the HadCM3LC climate-carbon cycle projection.

HadCM3LC produces a larger warming in the eastern equatorial Pacific than in the west (see Fig. 4a). This pattern is common to all previous and current Hadley Centre models, but appears strongest in 3rd generation models like HadCM3LC (Williams et al., 2001). Table 5 lists the terms contributing to the warming of the east and west Pacific regions. In the west there is a small reduction in cloud fraction (−0.04), but negligible change in the shortwave radiation fluxes. A much larger change can be seen in the downward longwave (29.2 W m$^{-2}$), which increases primarily because of $CO_2$-induced warming of the atmospheric column. The resulting increase in available energy is balanced by increases in the upward longwave (19 W m$^{-2}$) and latent heat fluxes (7.2 W m$^{-2}$), which both tend to increase in response to warming of the ocean surface.

There is a larger warming in the east (4.1 K versus 3.2 K in the west) but this is actually associated with a significant increase in cloud cover (0.15), and a significant decrease in downward shortwave radiation at the surface

**Table 5.** Change in surface energy balance (2090s–1990s) of the West Pacific (120° E–180° E, 5° S–5° N) and East Pacific regions (150° W– 90° W, 5° S–5° N), from the fully interactive climate-carbon cycle projection

| | West Pacific | East Pacific |
|---|---|---|
| Δ Screen Temperature (K) | 3.2 | 4.1 |
| Δ Cloud Fraction | −0.04 | 0.15 |
| Δ Downward Surface SW ($W m^{-2}$) | −0.7 | −16.7 |
| Δ Downward Surface LW ($W m^{-2}$) | 29.2 | 41.2 |
| Δ Upward Surface SW ($W m^{-2}$) | 0.0 | −0.8 |
| Δ Upward Surface LW ($W m^{-2}$) | 19.0 | 25.7 |
| Δ Latent Heat Flux ($W m^{-2}$) | 7.2 | 10.5 |
| Δ Sensible Heat Flux ($W m^{-2}$) | −0.1 | −0.7 |
| Δ Residual Heat Divergence ($W m^{-2}$) | 2.4 | −10.2 |

($-16.7\,W\,m^{-2}$). The downward longwave radiation increases by even more than it does in the western Pacific ($41.1\,W\,m^{-2}$ versus $29.2\,W\,m^{-2}$ in the west), most likely because of the ''blanket effect'' of increasing high clouds in the east. Dynamical processes in the ocean and atmosphere export heat from both regions, but this export changes more in the east Pacific where heat divergence (i.e. heat export) decreases by $10.2\,W\,m^{-2}$ as opposed to an increase of $2.4\,W\,m^{-2}$ in the west. As a result more energy is available to heat up the surface in the east, leading to larger warming and a greater enhancement of the upward longwave and latent heat fluxes.

This mechanism for a differential E–W warming seems quite different from that diagnosed in the NCAR GCM (Meehl and Washington, 1996), in which differential SW cloud feedbacks were implicated. It therefore seems the reasons for a relative warming of the east Pacific differ even amongst the subset of climate models that produce such a pattern. Whatever its cause, such an east–west variation in Equatorial Pacific SSTs is reminiscent of an El Niño state, in which similar SST patterns give rise to rainfall reductions in northern Brazil. So a key question is; could a long-term El Niño-like SST state give rise to rainfall reductions in Amazonia which could threaten the existence of the Amazonian rainforest?

Previous work has shown that HadCM3LC does a reasonable job in reproducing spatial and temporal patterns of ENSO variability and their impacts on the global carbon cycle (Jones et al., 2001). The parent HadCM3 model has been judged to be one of few GCMs in the Coupled Model Intercomparison project (CMIP) which is able to simulate recognisable NINO3 frequency spectra (AchutaRao and Sperber, 2002; Collins, 2001). Comparison to HadCM3 suggests that HadCM3LC, despite the lower oceanic horizontal resolution, has at least comparable ENSO performance. NINO3 anomalies have a standard deviation of around 0.8 K and have a broad peak in the spectra at periods of 3–6 years, both features which are quantitatively similar to that observed. In addition, and a likely consequence of the inclusion of the flux-correction term in HadCM3LC which corrects some of the errors in the mean climate in the region, the pattern of ENSO variability is more similar to the observed pattern than in the case of HadCM3. Deficiencies remain (for example an over correlation of land temperatures with NINO3 over tropical land), but HadCM3LC seems to be one of the more appropriate GCMs for the study of these links between El Niño and climate change.

This contention is broadly supported by Fig. 5 which compares the modelled and observed relationships between Amazonian rainfall and ENSO. Observed climate comes from the CRU dataset (New et al., 1999) and observed SSTs are from HadISST (Rayner et al., 2003). For both model and data SST indices are calculated over east Pacific NINO3 region: 150° W–90° W, 5° S–5° N, and over the west Pacific: 120° E–180° E, 5° S–5° N as December–February (DJF) mean SST and the difference (east–west) is taken as a measure of both interannual and longer term ENSO-like variability. The east–west SST gradient removes the effect of any mean global warming, which would be evident for example in the

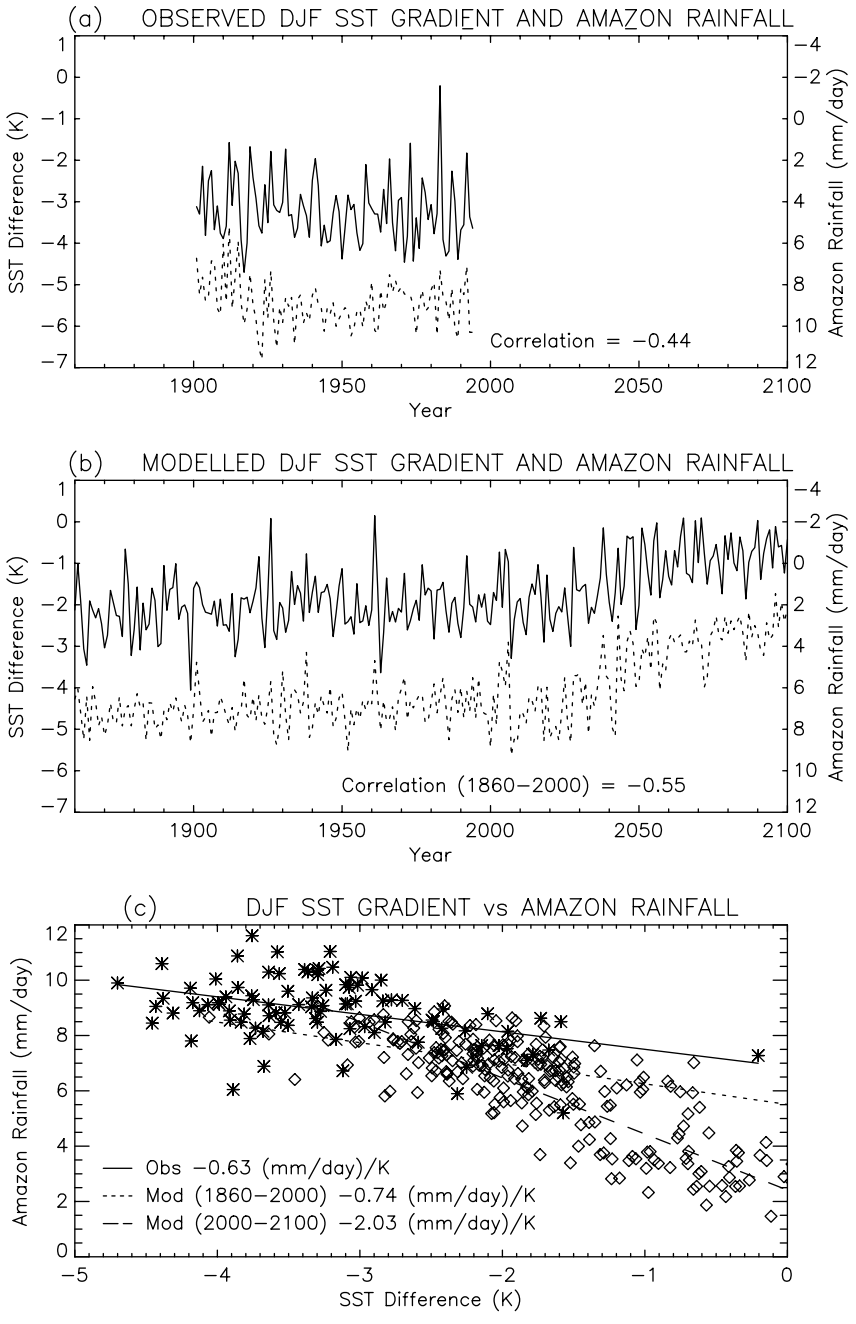


**Fig. 5.** Comparison of modelled and observed relationship between ENSO and Amazon rainfall. (**a**) Amazon rainfall (dashed line, right hand axis) and an east Pacific minus west Pacific SST index (thick line, left hand axis) against year from observational datasets, (**b**) Amazon rainfall and the same SST gradient index against year from the climate-carbon cycle model, (**c**) Amazon rainfall versus SST gradient index, Observed (asterixes) and Modelled (diamonds). Linear relationships are indicated for the model 1860–2000 and 2000–2100 periods, and for the observations

NINO3 index. The use of a SST gradient is more physically justifiable as it is directly related to the position of mean atmospheric convection which drives the teleconnection from the ENSO region to South America. Amazon rainfall is calculated as DJF (wet season) means over the region marked in Fig. 4 (70° W–50° W, 15° S–0° N). Comparing panels (a) and (b) of Fig. 5 note that the observations and model have similar interannual variability in both Amazonian rainfall and NINO3 index.

The model correctly reproduces the negative correlation between the ENSO SST difference and Amazonian rainfall on interannual time scales, matching the tendency for rainfall to be reduced during El Niño events. Indeed, the model seems to have a slightly higher correlation between the two variables although the observed estimate may be artificially low because of possible errors in the observations. The key feature of Fig. 5b is that this correlation is maintained for longer timescale trends so that as the pattern of

SSTs changes to a more ''El Niño-like'' mean pattern (still with the interannual variability present) the Amazonian rainfall correspondingly reduces. The amplitude of the relation on interannual time scales is slightly larger in the model for the period 1860–2000 ($-0.74\,\mathrm{mm\,day^{-1}\,K^{-1}}$) in comparison with the observations ($-0.63\,\mathrm{mm\,day^{-1}\,K^{-1}}$).

For the period 2000–2100 the model relationship strengthens to $-2.03\,\mathrm{mm\,day^{-1}\,K^{-1}}$, only partly because of local rainfall-vegetation feedback in Amazonia. The detailed mechanism for this stronger sensitivity is under investigation (using the atmospheric component of the model forced with different SST patterns). For the time being Fig. 5 can be considered as providing circumstantial evidence for a link between El Niño-like climate change and Amazonian climate change in HadCM3LC. As such, it suggests that study of the climate-carbon cycle system over natural ENSO cycles can provide valuable insights into the potential for Amazonian forest dieback under global warming.

## 6. Vegetation response to the projected climate change

Figure 6 shows the evolution of Amazonian land-cover from the fully coupled online simulation. It should be noted here that this run (and all others reported in this paper) ignore both direct anthropogenic deforestation and also natural fire disturbance. Nevertheless, as the Amazonian rainfall drops the broadleaf tree fraction is initially maintained at about 80% by direct $CO_2$ effects, but ultimately starts to reduce once the annual mean rainfall drops below a threshold of about $3\,\mathrm{mm\,day^{-1}}$ (see Fig. 7). The precise location of this rainfall threshold is dependent on the complexities of the soil-vegetation system under drying conditions, and it is therefore likely to be both uncertain and model-specific. However, the monotonic decrease in rainfall produced by this GCM would inevitably lead to forest dieback at some critical $CO_2$ level, regardless of the precise way in which these processes might be represented (i.e. no rainfall means no rainforest for all conceivable land-surface representations!).

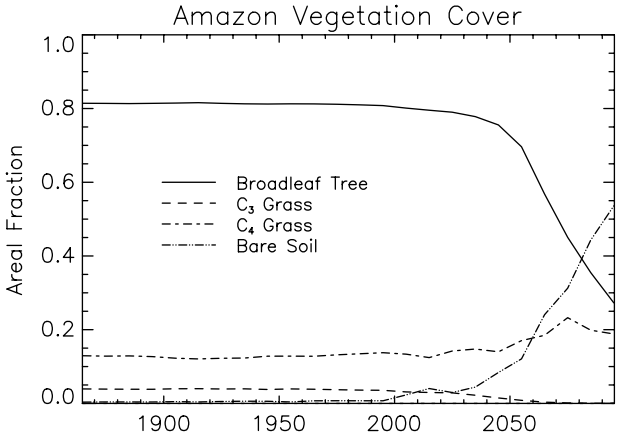


**Fig. 6.** Evolution of the vegetation cover in the Amazon box from the coupled climate-carbon cycle simulation

The mechanism of broadleaf tree dieback is the reduction of net primary productivity (NPP) below the levels necessary to maintain litter losses, which arise from both local processes (e.g. leaf-fall) and Lotka-type intraspecies competition (Cox, 2001). NPP reduces due to both soil moisture limitations on photosynthesis, and also increases in maintanence respiration costs (Cox et al., 1999). This version of TRIFFID assumes that leaf dark respiration and plant maintenance respiration increase exponentially with surface temperature, with a $q_{10}$ of 2 (Cox, 2001). The alternative assumption that respiration remains approximately proportional to photosynthesis even at high temperatures, acts to prevent NPP becoming negative and can delay forest dieback (Huntingford et al., 2000). However, once again such a modification can only influence the critical point at which dieback begins, since reducing NPP (as a result of moisture limitations) must ultimately make rainforest unsustainable.

When the forest fraction begins to drop (from about 2040 onwards) $C_4$ grasses initially expand to occupy some of the vacant lands. However, the relentless warming and drying make conditions unfavourable even for this plant functional type, and the Amazon box ends as predominantly bare-soil (area fraction $>0.5$) by 2100. As with the timing of dieback, the details of this simulation of the land-cover change should be treated with caution since they depend on known limitations and uncertainties in the TRIFFID vegetation model. For example, even at mean annual temperatures of approaching 40 °C a sparse cover of semi-desert CAM plants might be possible, but

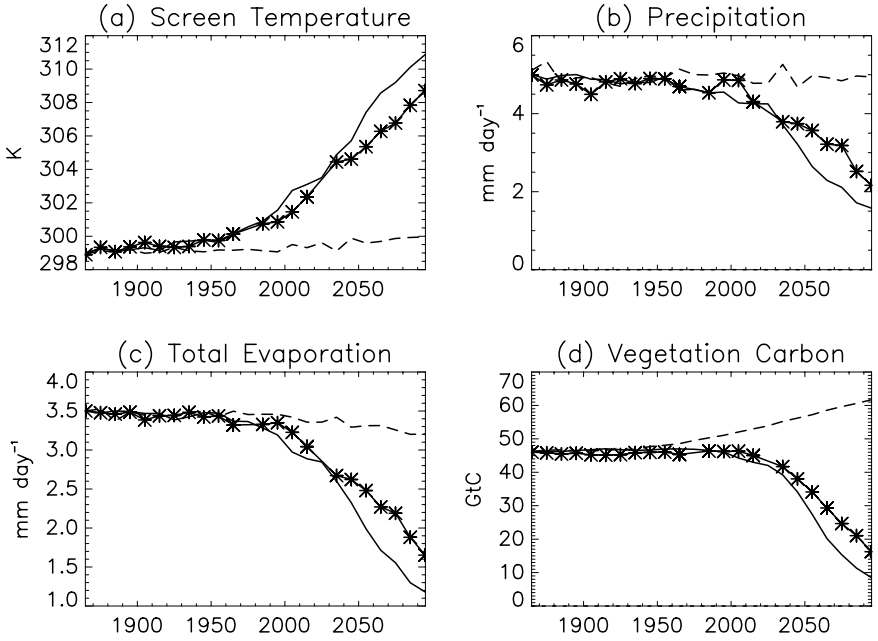


**Fig. 7.** Evolution of climate and biomass over the Amazon box, from three separate HadCM3LC simulations with dynamic vegetation. (**a**) Screen temperature, (**b**) precipitation, (**c**) evaporation, (**d**) vegetation carbon. The continuous line represents the fully coupled climate-carbon cycle run, the dashed line is from the run without climate effects on the carbon cycle, and the stars are from a run with prescribed IS92a $CO_2$ concentrations. The related $CO_2$ scenarios are shown in Fig. 1

this is not possible in TRIFFID since such heat and drought tolerant species are not recognised by the model. Despite these model deficiencies, it seems clear that the HadCM3LC climate change in Amazonia would lead to rainforest loss (perhaps via increased fire frequency), and therefore drastic land-cover change.

This assertion is backed-up by results from a comparison of dynamic global vegetation models (DGVMs), in offline experiments driven by output from the HadCM2 GCM (Cramer et al., 2001). An early offline version of TRIFFID (with simplfied surface energy balance and hydrology calculations) was amongst the 6 DGVMs used in this study. HadCM2 also produced a drying under high $CO_2$ in NE Brazil but this was less widespread than in HadCM3 or HadCM3LC. Nevertheless the DGVM intercomparison study does provide some insight into the dependence of the Amazonian dieback on the vegetation model details, since it subjected all DGVMs to the same climate change scenario. Figure 8 shows broadleaf tree biomass calculated over the Amazon box for simulations which excluded the direct effects of $CO_2$ on plant physiology. Each model was therefore subject to climate change impacts alone.

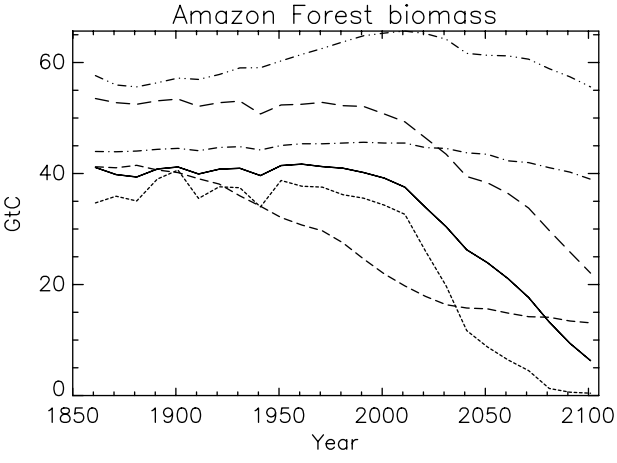


**Fig. 8.** Impact of climate change alone on Amazonian forest biomass in 6 different Dynamic Global Vegetation Models. In this particular experiment each DGVM was driven by the same climate change scenario from the HadCM2 GCM, but the direct effects of $CO_2$ on plant growth were excluded. Results from an early offline version of TRIFFID are shown as the continuous line

Although the detailed trajectories differ, there is a general tendency for Amazonian forest biomass to decrease through the 21st century as temperatures increase and rainfall drops (although less rapidly than in HadCM3LC). The most marked change was seen in the individual-based

gap model ''Hybrid'' (dotted line), which produced significant Amazonian dieback under both HadCM2 and HadCM3 scenarios even when direct $CO_2$ effects were included (Friend et al., 1997; White et al., 1999). The offline version of TRIFFID (continuous line in Fig. 8) projects a similar rate of carbon loss under climate change alone, but produced a stronger direct $CO_2$-effect which prevented such large-scale dieback under the HadCM2 scenario (Cramer et al., 2001). It therefore seems that DGVMs show a qualitatively similar tendency to reduce rainforest cover under a common scenario of warming and drying in Amazonia, but that the extent and rate of this reduction is model dependent. Reducing the uncertainty associated with vegetation model response to climate change will rely on making better use of field measurements to constrain process representations and internal model parameters (Harris et al., 2004).

## 7. Vegetation feedbacks on the climate change

Changes in land-cover can influence climate through a number of feedback loops. The potential for changes in land-carbon storage to feedback on climate by modifying the rate of atmospheric $CO_2$ increase was discussed in Section 4. However, land-cover also plays a large part in determining the surface-to-atmosphere heat, moisture and momentum fluxes, which in turn affect local energy balance (e.g. through changes in evaporative cooling and cloud cover) and the atmospheric circulation. Increased $CO_2$ tends to cause stomatal closure which acts to suppress transpiration and amplify surface warming (Cox et al., 1999), but increased leaf area index may counteract the reduced moisture flux per leaf area (Betts et al., 1997). Models of the climatic impacts of Amazonian deforestation yield a range of results, but generally indicate the potential for removal of the rainforest to produce less rainfall through reductions in moisture recycling and atmospheric moisture convergence (see for example Zeng et al. (1996) for a summary). Therefore, the climate change-driven deforestation in HadCM3LC might be expected to produce significant biophysical and biogeographical feedbacks.

A full analysis of vegetation feedbacks is provided by Betts et al. (2004). The impacts of forest dieback on the simulated Amazonian climate are briefly summarised here. In order to diagnose this two further GCM experiments were carried out, both using prescribed IS92a $CO_2$ concentrations to eliminate carbon cycle feedbacks. This scenario provides a trajectory of $CO_2$ which is very similar to that produced in the offline HadCM3LC experiment (see Fig. 1a), rising to a marginally higher concentration of 713 ppmv by 2100. One of the GCM experiments used fixed vegetation (equivalent to most existing GCM projections), while the other allowed for vegetation changes via TRIFFID. Figure 9 compares the evolution of the mean temperature, rainfall, evaporation and moisture convergence (P–E), from these two runs. In both cases the decadal mean screen-level temperature rises to about 309 K by the 2090s. By comparison the online run (which has much higher $CO_2$ by 2100) produced a 2090s temperature about 2 K higher (see Fig. 7a). The impacts of the dieback are more obvious in the Amazonian rainfall (Fig. 9b), with land-cover change producing an amplification of the drying in the last two decades of the 21st century. Decadal variability makes it difficult to estimate the magnitude of this effect with any certainty, but it appears to be up to 0.5 mm day$^{-1}$ by the 2090s, which is similar to the additional rainfall reduction arising from the extra $CO_2$ in the online run (see Fig. 7b).

Surprisingly, the runs with and without vegetation change produce remarkably similar evaporation rates (see Fig. 7c), possibly because soil moisture is so strongly limiting in the latter stages of both runs (such that vegetation change has a relatively small impact). In contrast the reducing forest cover has a clear impact on the rate at which moisture convergence reduces (Fig. 7d), with convergence reducing more quickly when vegetaion dynamics are included. The latter result is broadly consistent with the thermodynamic analysis of Amazonian deforestation by Zeng et al. (1996), which suggests that precipitation and moisture convergence will both decrease approximately linearly with reducing evaporation.

In HadCM3LC forest dieback is therefore acting to amplify the Amazon drying which causes it, and is therefore involved in the propagation of

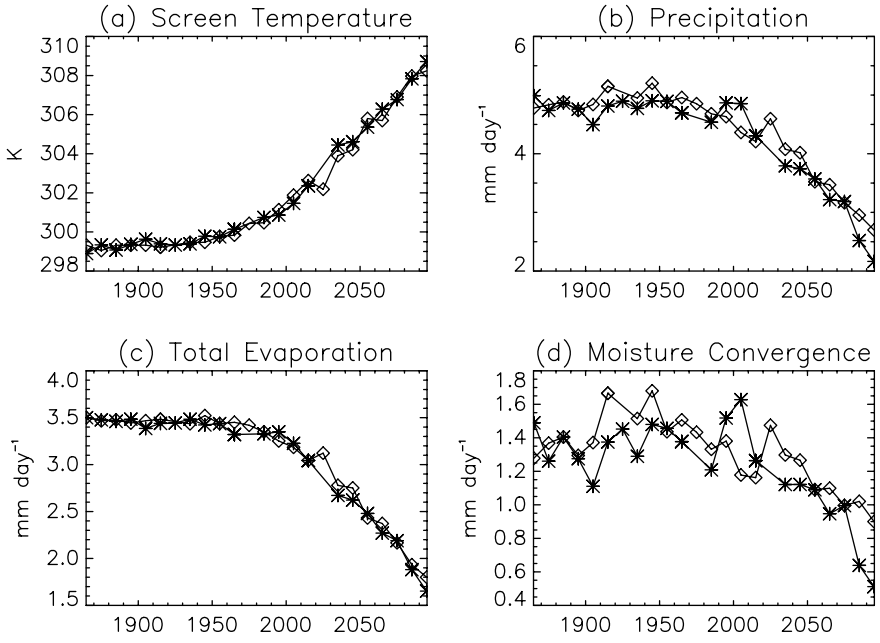


**Fig. 9.** Evolution of climate and hydrology over the Amazon box, from 2 separate HadCM3LC simulations with prescribed IS92a $CO_2$ concentrations. (**a**) Screen temperature, (**b**) precipitation, (**c**) evaporation, (**d**) moisture convergence (P–E). The stars are from a run with dynamic vegetation and the diamonds are from a run with fixed vegetation

the drying pattern from east to west (Betts et al., 2004). However, vegetation feedbacks are not the primary drivers for the drying, since this occurs even in the HadCM3LC experiment which has prescribed $CO_2$ and fixed vegetation.

## 8. Discussion

The analysis presented in this paper provides a qualitative explanation of the Amazonian forest dieback phenomenon in the Hadley Centre climate carbon cycle model. Further work is required to relate the model to aspects of the real Earth system which would allow us to quantify the probability of climate-driven forest dieback in Amazonia. In this section some of the key scientific questions are listed, along with some tentative answers and suggestions based on the results presented in this paper.

(i) What is the mechanism of Amazonian drying in the Hadley Centre's climate-carbon cycle model?

Our analysis suggests that the primary cause of Amazonian climate change is the El Niño-like SST warming pattern which emerges in HadCM3LC as $CO_2$ increases. $CO_2$-induced stomatal closure also acts to warm and dry the Amazon basin, adding slightly to the regional climate change (Betts et al., 2004; Cox et al., 1999). The Amazonian drying leads ultimately to forest dieback which releases $CO_2$ to the atmosphere, contributing about one tenth to the $CO_2$ amplification by 2100, and further reducing rainfall over Amazonia (by about $0.5\,\mathrm{mm\,day^{-1}}$) through changes in the properties of the land-surface. Further analysis is required to quantify the contributions of the various physical and biological feedbacks to the overall model response.

(ii) How realistic is the El Niño-like drying pattern in Amazonia as $CO_2$ increases?

All of the third generation Hadley Centre models tend to produce greater warming in the tropical eastern Pacific than the west (i.e. an El Niño-like mean SST pattern), leading to reductions in rainfall along the northeast coast of South America. A number of other GCMs produce a similar SST warming pattern (IPCC, 2001), but this is by no means common to all models. Figure 10 shows a simple estimate of current uncertainty in east–west SST gradient change and Amazon rainfall change in all models submitted to Phase 2 of the Coupled Model Intercomparison project (CMIP2 Covey et al. (2003) – http://www-pcmdi.llnl.gov/cmip). There is a tendency for the models to fall around a diagonal with drying conditions in Amazonia associated with a warming of the tropical

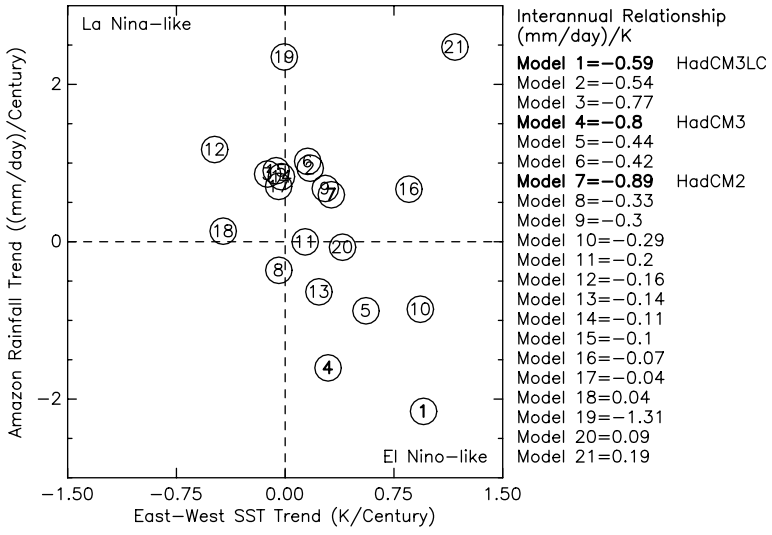


**Fig. 10.** Century time scale trends in DJF mean east–west SST gradient versus DJF mean Amazon rainfall (regions defined in Fig. 5) from 20 model simulations submitted to the Coupled Model Intercomparison Project (CMIP2) in which $CO_2$ is increased at the rate of 1% per year (compounded) plus HadCM3LC. To make a more fair comparison, the HadCM3LC response is taken from years 2000–2080 of a simulation with IS92a $CO_2$ and fixed vegetation (in the simulation with interactive vegetation the rainfall reduction is approximately twice the value with fixed vegetation). The models are numbered according to how well they reproduce the interrannual relationship between SST gradient and Amazon rainfall which is indicated in the table to the right of the figure. The Hadley Centre models are marked in bold, with HadCM3LC ranked as number 1

east Pacific relative to the west, and increased rainfall associated with a relative warming of the west, but the scatter is significant. The models have been numbered according to the realism with which each simulates the interannual relationship between SST gradient and Amazonian rainfall. HadCM3LC has the strongest positive trend in the E–W SST contrast associated with the strongest negative trend in Amazonian rainfall, but it is also the model which most closely matches the observed interannual relationship between these variables (the slope of the relationship is slightly different from that shown in Fig. 5 as this is computed from the HadCM3LC control, not years 1860–2000 of the transient run).

The mechanism for the El Niño-like SST pattern in HadCM3LC appears to be related to differential cloud feedbacks in the eastern and western Pacific, enhanced by coupled ocean-atmosphere dynamics, as similar patterns are seen when the atmospheric component is coupled to a thermodynamic slab ocean (Williams et al., 2001). Note also that the use of flux-adjustments in HadCM3LC appears not to have played a critical role in the development of such a ''permanent El Niño'', since a similar pattern of warming is seen in the unflux-adjusted HadCM3 model (Model 4 in Fig. 10).

The similarity of the climate change pattern to an El Niño state offers some hope of validating some of the key model sensitivities using data on interannual variability. A previous study has shown that HadCM3LC can reproduce ENSO variability and the related global carbon cycle response with reasonable accuracy (Jones et al., 2001), thus providing a constraint on a key internal model parameter (Jones and Cox, 2001). A key area for future research should be in relating interannual data and results from other models to allow some estimate of the uncertainty bounds on the response of Amazon rainfall to an El Nino-type SST anomaly.

(iii) How realistic is the vegetation model response to the simulated Amazon drought? The extent of the projected warming and drying of Amazonia (10 K warming plus a 60+% rainfall reduction by 2100) inevitably makes the rainforest unsustainable. However, the threshold for forest dieback is undoubtedly vegetation-model dependent

and therefore uncertain. The TRIFFID assumption that plant maintenance respiration increases with temperature makes the rainforest less robust to warming than it might be (Huntingford et al., 2000), but the neglect of forest fire probably makes the modelled vegetation more robust to drying than it is in reality. The HadCM3LC model also underestimates the rainfall in present-day Amazonia by about 20%, such that any thresholds in rainfall are likely to be passed earlier (and at lower $CO_2$ concentrations) than they might be in the real Earth system (Huntingford et al., 2004). Nevertheless, the magnitude of the Amazonian climate change in HadCM3LC seems sure to lead to eventual loss of rainforest in all vegetation models, as suggested by an offline intercomparison of DGVMs (Cramer et al., 2001).

The increasing availability of $CO_2$ flux data offers the possibility of refining and validating vegetation models to a new level, thereby providing more robust projections of the response of the Amazonian forest to an imposed climate change (Harris et al., 2004). In addition, artificial droughting experiments and observational campaigns during El Niño events, can provide valuable information on the response of real forest ecosystems to moisture stress.

## 9. Conclusions

This paper has summarised the phenomenon of Amazonian forest dieback within climate change projections carried out with the Hadley Centre climate-carbon cycle GCM. In this model, high $CO_2$ leads to an El-Nino-like SST warming pattern which suppresses rainfall across northern Amazonia. Although $CO_2$-fertilisation of photosynthesis is able to maintain the rainforest cover for the first half of the 21st century, the extreme warming and drying eventually lead to abrupt reductions in the forest fraction. The loss of rainforest exacerbates the Amazonian climate change by releasing $CO_2$ to the atmosphere, and by changing the properties of the land-surface.

The modelled Amazonian dieback phenomenon is therefore qualitatively understood, but we are still a long way from being able to estimate the probability of such an ecological catastrophy occurring in the real Earth system. Further progress on this issue will rely on analysing results from a range of GCMs and vegetation models (e.g. as part of the Coupled Climate-Carbon Cycle Model Intercomparison Project, ''$C^4$MIP''), each validated more thoroughly with the latest observational data. This research is urgently required if we are to provide useful guidance on potentially dangerous levels of $CO_2$ for the rainforest of Amazonia.

**Acknowledgements**

The authors of this work were supported by the UK DETR Climate Prediction Programme under contract PECD 7/12/37 (Peter Cox, Richard Betts and Chris Jones), and the Natural Environment Research Council (Matthew Collins, Phil Harris, and Chris Huntingford).

**References**

AchutaRao K, Sperber KR (2002) Simulation of the El Nino Southern Oscillation: results from the Coupled Model Intercomparison Project. Climate Dynamics 19: 191–210

Bacastow R, Keeling C (1981) Atmospheric $CO_2$ and the southern oscillation: effects associated with recent El Nino events. In WMO/ICSU/UNEP Scientific Conference on analysis and interpretation of atmospheric $CO_2$ data WMO, World Clim. Prog. Off., Geneva vol. WCP 14 of *World Climate Programme*

Betts RA, Cox PM, Collins M, Harris PP, Huntingford C, Jones CD (2004) The role of ecosystem-atmosphere interactions in simulated Amazonian precipitation decrease and forest dieback under global climate warming. Theor Appl Climatol (this issue)

Betts RA, Cox PM, Lee SE, Woodward FI (1997) Contrasting physiological and structural vegetation feedbacks in climate change simulations. Nature 387: 796–799

Collatz GJ, Ball JT, Grivet C, Berry JA (1991) Physiological and environmental regulation of stomatal conductance, photosynthesis and transpiration: A model that includes a laminar boundary layer. Agric Forest Meteorol 54: 107–136

Collatz GJ, Ribas-Carbo M, Berry JA (1992) A coupled photosynthesis-stomatal conductance model for leaves of $C_4$ plants. Aus J Plant Physiol 19: 519–538

Collins W (2001) Effects of enhanced shortwave absorption on coupled simulations of the tropical climate system. J Clim 14: 1147–1165

Covey C, AchutaRao KM, Cubash C, Jones P, Lambert SJ, Mann ME, Phillips TJ, Taylor KE (2003) An overview of results from the Coupled Model Intercomparison Project (CMIP). Global and Planetary Change 37: 103–133

Cox PM (2001) Description of the TRIFFID Dynamic Global Vegetation Model. Technical Note 24 Hadley Centre, Met Office

Cox PM, Betts RA, Bunton CB, Essery RLH, Rowntree PR, Smith J (1999) The impact of new land surface physics on the GCM simulation of climate and climate sensitivity. Clim Dyn 15: 183–203

Cox PM, Betts RA, Jones CD, Spall SA, Totterdell IJ (2000) Acceleration of global warming due to carbon-cycle feedbacks in a coupled climate model. Nature 408: 184–187

Cox PM, Betts RA, Jones CD, Spall SA, Totterdell IJ (2001) Modelling vegetation and the carbon cycle as interactive elements of the climate system. In: Pearce R (ed) Meteorology at the millennium. Academic Press, pp 259–279

Cox PM, Huntingford C, Harding RJ (1998) A canopy conductance and photosynthesis model for use in a GCM land surface scheme. J Hydrology 212–213: 79–94

Cramer W, Bondeau A, Woodward F, Prentice I, Betts R, Brovkin V, Cox P, Fisher V, Foley J, Friend A, Kucharik C, Lomas M, Ramankutty N, Stitch S, Smith B, White A, Young-Molling C (2001) Global response of terrestrial ecosystem structure and function to $CO_2$ and climate change: Results from six dynamic global vegetation models. Global Change Biol 7(4): 357–374

DOE (1994) Handbook of methods for the analysis of the various parameters of the carbon dioxide system in sea water; version 2 U.S. DOE

Essery RLH, Best MJ, Betts RA, Cox PM, Taylor CM (2003) Explicit representation of subgrid heterogeneity in a GCM land-surface scheme. J Hydromet 4(3): 530–543

Field C, Jackson R, Mooney H (1995) Stomatal responses to increased $CO_2$: implications from the plant to the global scale. Plant, Cell and Environment 18: 1214–1225

Friedlingstein P, Bopp L, Ciais P, Dufresne J, Fairhead L, LeTreut H, Monfray P, Orr J (2001) Positive feedback between future climate change and the carbon cycle. Geophys Res Lett 28(8): 1543–1546

Friend AD, Stevens AK, Knox RG, Cannell MGR (1997) A process-based, terrestrial biosphere model of ecosystem dynamics (Hybrid v3.0). Ecological Modelling 95: 249–287

Gedney N, Cox P, Douville H, Polcher J, Valdes P (2000) Characterizing GCM land-surface schemes to understand their responses to climate change. J Clim 13: 3066–3079

Giardina C, Ryan M (2000) Evidence that decomposition rates of organic carbon in mineral soil do not vary with temperature. Nature 404: 858–861

Gordon C, Cooper C, Senior CA, Banks H, Gregory JM, Johns TC, Mitchell JFB, Wood RA (2000) The simulation of SST, sea ice extents and ocean heat transports in a version of the Hadley Centre coupled model without flux adjustments. Clim Dyn 16: 147–168

Harris PP, Huntingford C, Gash JHC, Hodnett M, Cox PM, Malhi Y, Araujo AC (2004) Calibration of a land-surface model using data from primary forest sites in Amazonia. Theor Appl Climatol (this issue)

Huntingford C, Cox P, Lenton T (2000) Contrasting responses of a simple terrestrial ecosystem model to global change. Ecological Modelling 134: 41–58

Huntingford C, Harris PP, Gedney N, Cox PM, Betts RA, Gash JHC, Marengo J (2004) Using a GCM analogue model to investigate the potential for Amazonian forest "dieback" in a future climate. Theor Appl Climatol (this issue)

IPCC (2001) Climate Change 2001: The Scientific Basis. Contribution of Working Group I to the Third Assessment Report of the Intergovernmental Panel on Climate Change Cambridge, United Kingdom and New York, NY, USA: Cambridge University Press, 881pp

Jenkinson DS, Adams DE, Wild A (1991) Model estimates of $CO_2$ emissions from soil in response to global warming. Nature 351: 304–306

Jones C, Cox P (2001) Constraints on the temperature sensitivity of global soil respiration from the observed interannual variability in atmospheric $CO_2$. Atmospheric Science Letters p. doi: 10.1006/asle.2000.0041

Jones CD, Collins M, Cox PM, Spall SA (2001) The carbon cycle response to ENSO: A coupled climate-carbon cycle model study. J Clim 14(21): 4113–4129

Jones CD, Cox PM, Essery RLH, Roberts DL, Woodage MJ (2003) Strong carbon cycle feedbacks in a climate model with interactive $CO_2$ and sulphate aerosols. Geophys Res Lett 30(9): 10.1029/2003GL016867

Lean J, Rowntree PR (1993) A GCM simulation of the impact of Amazonian deforestation on climate using an improved canopy representation. Quart J Roy Meteor Soc 119: 509–530

Lean J, Rowntree PR (1997) Understanding the sensitivity of a GCM simulation of Amazonian deforestation to the specification of vegetation and soil characteristics. J Climate 10(6): 1216–1235

Loveland TR, Reed BC, Brown JF, Ohlen O, Zhu Z, Yang L, Merchant JW (2000) Development of a global land cover characteristics database and IGBP DISCover from 1 km AVHRR data. Int J Remote Sens 21: 1303–1330

Meehl GA, Washington WM (1996) El Niño-like climate change in a model with increased atmospheric $CO_2$ concentrations. Nature 382: 56–60

Nepstad DC, Verssimo A, Alencar A, Nobre C, Lima E, Lefebvre P, Schlesinger P, Potter C, Moutinho P, Mendoza E, Cochrane M, Brooks V (1999) Large-scale impoverishment of Amazonian forests by logging and fire. Nature 398: 505–508

New M, Hulme M, Jones P (1999) Representing twentieth century space-time climate variability. 1: Development of a 1961–1990 mean monthly terrestrial climatology. J Climate 12(3): 829–856

Palmer JR, Totterdell IJ (2001) Production and export in a global ocean ecosystem model. Deep-Sea Res 48(5): 1169–1198

Peng TH (1987) Seasonal variability of carbon dioxide, nutrients and oxygen in the northern North Atlantic surface water: observations and a model. Tellus 39B: 439–458

Raich J, Schlesinger W (1992) The global carbon dioxide flux in soil respiration and its relationship to vegetation and climate. Tellus 44B: 81–99

Rayner NA, Parker DE, Horton EB, Folland CK, Alexander LV, Rowell DP, Kent EC, Kaplan A (2003) Global analyses of SST, sea ice and night marine air temperature since the late nineteenth century. J Geophys Res 108(D14): 10.1029/2002JD002670

Schimel D, Alves D, Enting I, Heimann M, Joos F, Raynaud D, Wigley T, Prather M, Derwent R, Enhalt D, Fraser P, Sanhueza E, Zhou X, Jonas P, Charlson R, Rodhe H, Sadasivan S, Shine KP, Fouquart Y, Ramaswamy V, Solomon S, Srinivasan J, Albritton D, Derwent R, Isaksen I, Lal M, Wuebbles D (1996) Radiative forcing of climate change. In: Houghton JT, Filho LGM, Callander BA, Harris N, Kattenberg A, Maskell K (eds) Climate change 1995. The Science of Climate Change. Cambridge: Cambridge University Press, chap 2, pp 65–131

Sellers PJ, Bounoua L, Collatz GJ, Randall DA, Dazlich DA, Los SO, Berry JA, Fung I, Tucker CJ, Field CB, Jensen TG (1996) Comparison of radiative and physiological effects of doubled atmospheric $CO_2$ on climate. Science 271: 1402–1406

Wanninkhof R (1992) Relationship between wind speed and gas exchange over the ocean. J Geophys Res 97: 7373–7382

White A, Cannell M, Friend A (1999) Climate change impacts on ecosystems and on the terrestrial carbon sink: a new assessment. Global Environ Change 9: S21–S30

Williams KD, Senior CA, Mitchell JFB (2001) Transient climate change in the Hadley Centre models: The role of physical processes. J Clim 14(12): 2659–2674

Zeng N, Dickinson R, Zeng X (1996) Climatic impact of Amazon deforestation – a mechanistic model study. J Clim 9: 859–883

Authors' addresses: Peter Cox (e-mail: peter.cox@metoffice. com), R. A. Betts and C. D. Jones, Hadley Centre for Climate Prediction and Research, Met Office, Exeter EX1 3PB, U.K.; M. Collins, Department of Meteorology, University of Reading, Reading, Berks, U.K.; P. P. Harris and C. Huntingford, Centre for Ecology and Hydrology, Wallingford, Oxon OX10 8BB, U.K.